Characterizing Prion-Like Protein Aggregation: Emerging Nanopore-Based Approaches

Nathan Meyer, Joan Torrent, Sébastien Balme

small methods
www.small-methods.com

Characterizing Prion-Like Protein Aggregation: Emerging Nanopore-Based Approaches

*Nathan Meyer, Joan Torrent, and Sébastien Balme**

Prion-like protein aggregation is characteristic of numerous neurodegenerative diseases, such as Alzheimer's and Parkinson's diseases. This process involves the formation of aggregates ranging from small and potentially neurotoxic oligomers to highly structured self-propagating amyloid fibrils. Various approaches are used to study protein aggregation, but they do not always provide continuous information on the polymorphic, transient, and heterogeneous species formed. This review provides an updated state-of-the-art approach to the detection and characterization of a wide range of protein aggregates using nanopore technology. For each type of nanopore, biological, solid-state polymer, and nanopipette, discuss the main achievements for the detection of protein aggregates as well as the significant contributions to the understanding of protein aggregation and diagnostics.

1. Introduction

Prion-like protein aggregation is a common characteristic of numerous neurodegenerative diseases, including Alzheimer's and Parkinson's diseases.[1] This three-phase process involves the formation of aggregates ranging from small and potentially neurotoxic oligomers to highly structured self-propagating amyloid fibrils.[2] The first phase, known as the lag phase, involves the formation of small aggregates of misfolded proteins, which exhibit diverse structures and lower growth rates than fibrils.[3] These oligomers are considered metastable and can be either on- or off-pathway. In the second phase, called the growing phase, on-pathway oligomers grow to form protofibrils and fibrils highly structured β-sheets.[4] Finally, the aggregation process reaches a plateau, where the majority of the monomers are in fibrillar form (**Figure 1**). In recent years, considerable research has been devoted to understanding the mechanism of protein aggregation, particularly in the early stages, which are not yet fully understood due to the low concentration, and highly heterogeneous structure.[5] Indeed, the species formed during this phase are soluble oligomers that are mostly unorganized into β-sheet structures, making them undetectable by ThT fluorescence emission. These soluble oligomers appear to trigger the aggregation process and the amyloid cascade. Moreover, research has suggested that they are the most toxic to neurons.[6] Oligomer formation during the initial phase was highly complex. These entities are poorly characterized owing to their metastable nature in solution.[7] However, experimental studies coupled with theoretical kinetic models have revealed the biochemical mechanisms of their production.[8] The aggregation process involves interconnected phenomena, starting with a primary nucleation step, where non-fibrillar oligomers known as "off-pathways" are formed and then reorganized into oligomers capable of forming a fiber ("on-pathways"). In fact, only fibrillar oligomers will be stable enough to produce an amyloid fiber. Once produced, the latter can catalyze the formation of new fibrillar oligomers on its surface. This phenomenon, known as secondary nucleation, is responsible for the rapid proliferation of β-sheet-rich structures observed during the exponential aggregation phase (**Figure 2c**).[3] Two distinct nucleation mechanisms lead to the formation of fibrillar structures during the early phases.[9] The primary nucleation mechanism corresponds to the formation of fibrillar oligomers following self-aggregation (Figure 2c, top). In the second mechanism, known as secondary nucleation, the fibers formed by primary nucleation act as a catalytic surface for the peptide, facilitating its aggregation.

Over the years, various approaches have been developed to study the early stages of protein aggregation. These include monitoring the depletion of monomers and the formation of aggregate structures.[3] The most commonly used technique for monitoring the aggregation kinetics is the enhancement of Thioflavine T (ThT) fluorescence, which binds to the characteristic β-sheet structures of amyloid.[10] Nuclear magnetic resonance (NMR) spectroscopy in solution was used to study the evolution of the monomer concentration over time (Figure 2a).[11] In contrast, solid-state NMR (ssNMR) is suitable for resolving the structure of amyloid fibers harvested in the plateau phase.[12] Fourier Transform Infrared (FTIR) spectroscopy can

N. Meyer, S. Balme
Institut Européen des Membranes
UMR5635 University of Montpellier ENCSM CNRS
Place Eugène Bataillon, Cedex 5, Montpellier 34095, France
E-mail: sebastien.balme@umontpellier.fr
N. Meyer, J. Torrent
INM
University of Montpellier
INSERM
Montpellier 34095, France

The ORCID identification number(s) for the author(s) of this article can be found under https://doi.org/10.1002/smtd.202400058

DOI: 10.1002/smtd.202400058

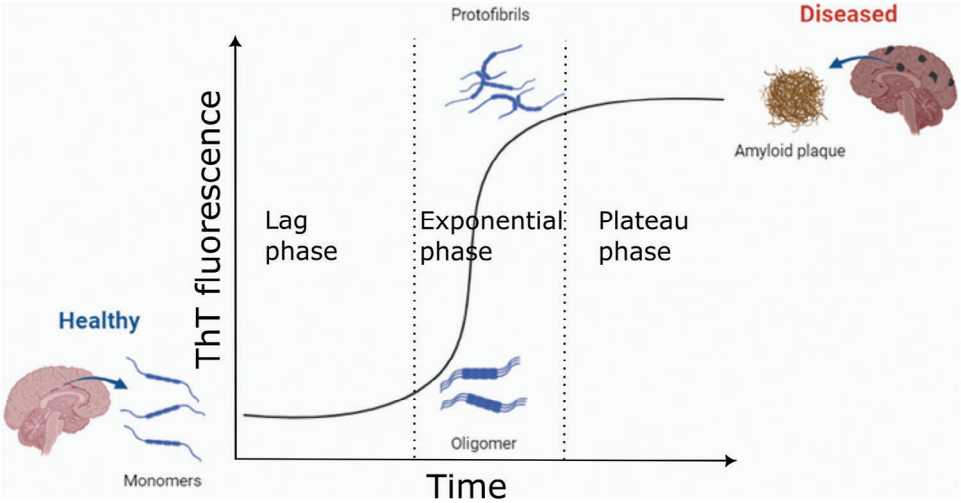

Figure 1. Diagram of amyloid protein aggregation. The kinetics follow a sigmoidal pattern, which can be broken down into 3 phases (lag, exponential, plateau). The species present in the lag phase, mainly oligomers, are insensitive to Thioflavin T, as they are not structured into β-sheets. At the end of the aggregation process (plateau), the fibers are organized into plaques, which are responsible for various neurodegenerative diseases.

be used to monitor the concentration of aggregates[13] and the secondary structure through the analysis of the amide I absorption band between 1600 and 1700 cm^{-1}.[14] Similarly, Raman spectroscopy allows differentiating between different fibril morphologies and toxic oligomers.[15] Circular dichroism (CD) can be used to characterize and quantify different secondary structure elements, allowing the monitoring of conformational changes during the aggregation process (Figure 2b).[16] However, these techniques only provide averaged information about the sample, and none about specific polymorphic, transient, and heterogeneous species that co-exist during the aggregation process.[17] Single-molecule techniques are powerful tools for identifying different proteomorphs and elucidating the complex mechanisms of aggregation processes. These methods primarily rely on fluorescence techniques such as Förster resonance energy transfer (FRET) and fluorescence correlation spectroscopy (FCS) in solution.[18] Confocal fluorescence spectroscopy, in which photons emitted by ThT or another fluorescent molecule from an oligomer passing through a confocal volume are detected, allows in situ monitoring of aggregation (Figure 2c).[19] After chromatographic separation, absorbance or radioactivity measurements can be used to quantify oligomers, while mass spectrometry can provide information on the number of monomers in an aggregate.[9,20] Transmission electron microscopy (TEM) provides information on the morphology of the species, while cryo-electron microscopy (CryoEM) is useful for determining the molecular architecture of the fibrils.[21] Atomic force microscopy (AFM) has been used to characterize the topography of the various species formed during aggregation[22] and the mechanical properties of the fibrils.[23] The development of high-speed AFM has made it possible to observe fiber growth in real-time.[24]

Although the techniques discussed in the previous section allow the study of monomers and fibrils over time, they are not suitable for the direct characterization of oligomers in solution. Furthermore, early phase oligomers are insensitive to intercalating agents, such as ThT, yet, the early stages of protein aggregation have a significant impact on various diseases. Despite advancements in characterization techniques, there are several unanswered questions regarding the composition of small and transient oligomers not structured in β-sheets, such as i) how the ratio between the soluble oligomer and the one structured in β-sheet structure influences the onset of the exponential phase, ii) how external factors like shaking, temperature, drugs, and pollutants affect the size, shape, distribution, and concentration of the soluble oligomer, or iii) which species are produced through secondary nucleation mechanisms. The time and monomer concentration required for a sample to be sensitive to ThT are significant limitations to the development of real-timequaking Induced Convertion- (RT-QuIC) as a diagnostic tool. Directly probing oligomers before their structuration in β-sheet-rich fibrils may be a promising approach for the development of early diagnostic assays. In summary, there is a strong need for a novel approach, particularly to characterize the morphology of small oligomers under continuous conditions. Understanding the formation mechanisms of these oligomers may pave the way for the development of novel therapeutic and diagnostic tools. Among emerging approaches, nanopores can complement the existing panel of techniques. Nanopores allow the characterization of a single macromolecule, providing information on its sequence, structure, volume, and folding state. They can detect small peptides as well as aggregates of several hundred nanometers without labeling by choosing a nanopore size of the same order as the analyte. Although nanopores are inherently non-selective, their functionalization can make them specific to a particular species. This review provides an up-to-date overview of emerging nanopore-based approaches for the detection and characterization of protein aggregates.

2. Nanopore Sensing

The emergence of nanopore technology in the 1990s resulted in remarkable achievements in real-time, label-free, and single-molecule DNA sequencing.[25] However, this technology has

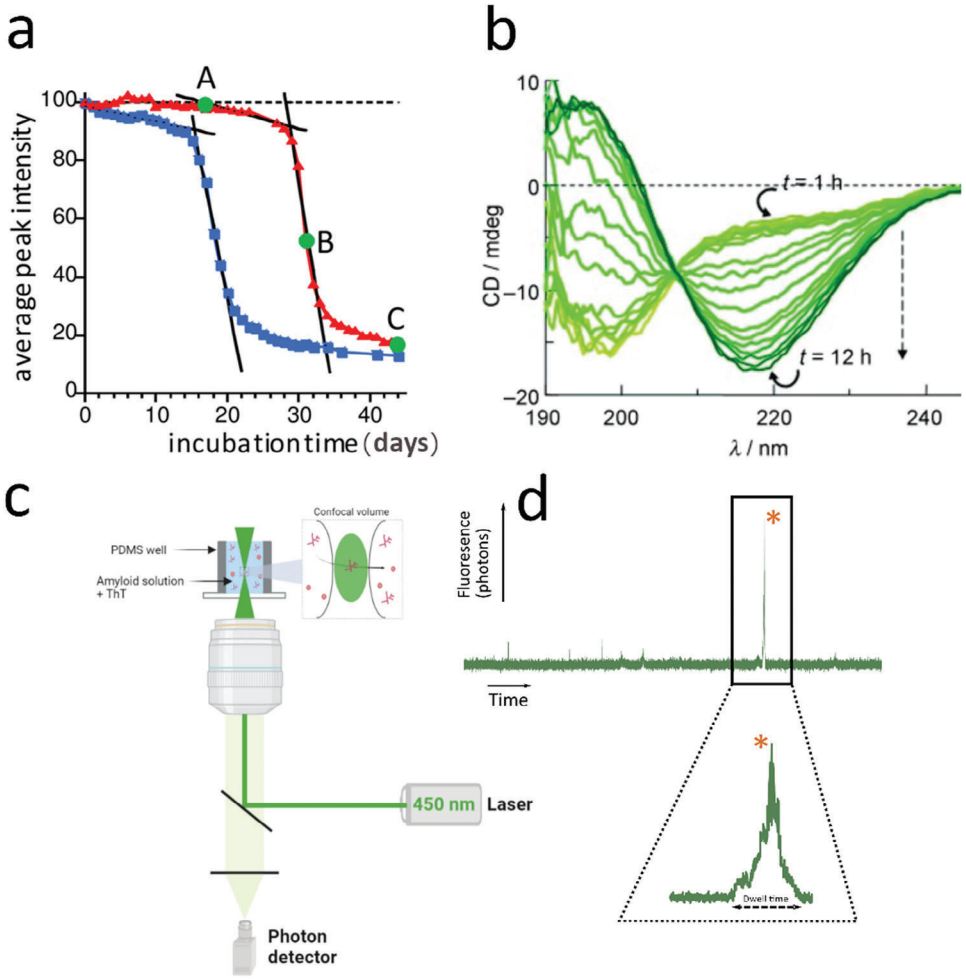

Figure 2. a) Intensity of the peak corresponding to the amide and aromatic regions monitored by NMR as a function of time. With time, the intensity decreases, indicating aggregation. The blue and red curves correspond to aggregation of IAPP (amyloid protein) in the absence and presence of curcumin respectively. Figure adapted from.[11a] Copyright 2012, American Chemical Society b) Superimposed DC spectra recorded at 45-min time intervals. The increase in the amount of amyloid–β is indicated by the increase in a negative band at 215 nm and a positive band at 195 nm. Figure adapted from.[16b] Copyright 2007, Wiley c) Experimental diagram of a device for detecting amyloid aggregates by confocal spectroscopy. d) fluorescence photons as a function of time measured, when a ThT-bound aggregate passes through the volume, a burst of fluorescence is measured. The properties of this burst, in particular its duration, provide information on the properties of the aggregate that has passed through the confocal volume (its diffusion coefficient, friction coefficient, etc.).

also been extended to other analytes such as metal ions, small molecules, proteins, nanoparticles, and amyloids.[26] Single-molecule detection using nanopore technology is based on the resistive pulse principle (**Figure 3**).[27] Specifically, a nanometric hole (nanopore) is positioned between two reservoirs filled with an electrolyte solution (such as NaCl or KCl). By applying a voltage between the two electrodes immersed in the reservoirs, the movement of electrolytes and fluids through the nanopore is induced, generating a constant ionic current (I_0) that is measured as a function of time. When an analyte passes through the nanopore, the current perturbation is measured (as shown in Figure 3, right panel). The amplitude of the current perturbation (ΔI) provides information about the volume and shape of the analyte. In general, the larger the volume of the analyte, the greater the resulting ΔI.[28] However, it is important to note that the charge of the analyte can also affect the ΔI at low salt concentrations due to the presence of counterions on their surface. Consequently, the two analytes with similar volumes but different charges may display different ΔI values.[29] Another commonly used parameter is the dwell time (Δt). Although it can provide information on analyte parameters,[30] it is often more difficult to interpret.[31] The dwell time depends on the diffusion coefficient of the analyte and its apparent charge inside the nanopore, which may differ from that of the bulk.[32] In addition, the dwell time is influenced by the interaction between the analyte and the nanopore, such as transient adsorption or target/probe transient binding, the energy barrier for the entrance and exit of the analyte as well as the electroosmotic flow.[33] Consequently, the dwell time is more difficult to estimate than the blockade amplitude. The frequency of the current perturbation also depends on the analyte concentration, its diffusion coefficient in the bulk, and the energy barrier.[34]

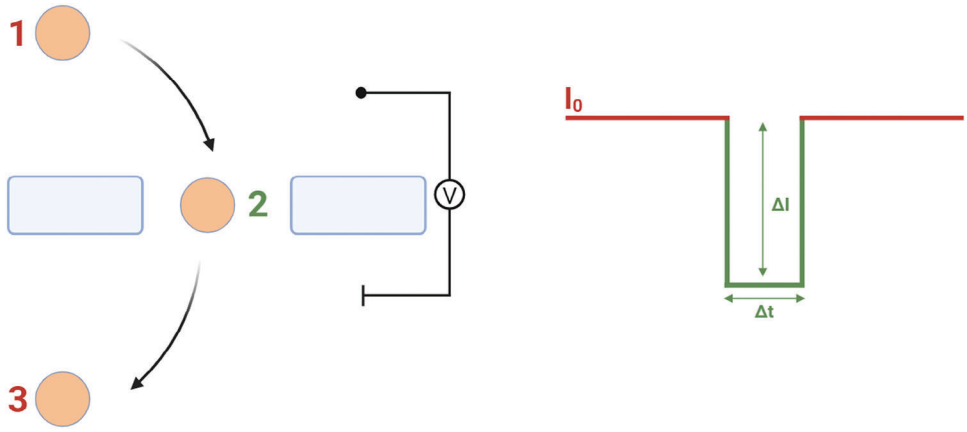

Figure 3. Left, experimental principle of the resistance pulse. Right, schematic representation of current blockage when an analyte passes through the pore. The current I_0 corresponds to the open pore, and ΔI corresponds to the current blockage when a molecule transiently blocks the pore. Δt corresponds to the duration of current blockage.

2.1. Biological Nanopore for "Prion-Like" Protein Sensing

Biological nanopores are transmembrane channels with diameters ranging from 1 to 4 nm,[35,25a,36] and have been used for biomolecule sensing since the pioneering work involving a nanopore demonstrated the detection and discrimination of polynucleotides using the α-hemolysin toxin produced by the bacterium Staphylococcus Aureus. Subsequently, biological nanopores were developed using a porin from Mycobacterium smegmatis (MspA) or those formed by a toxin present in Aeromonas hydrophila (Aerolysin) (**Figure 4a**). Their precise structure makes them suitable for sequencing applications, as well as for the analysis of biomolecular modifications induced by radioactive or enzymatic reactions, or the identification of targets associated with disease. They have also been widely used to study unfolded proteins.[37] Currently, the most ambitious goal for biological nanopores is protein sequencing, which is more challenging than DNA sequencing because of the 22 proteinogenic amino acids (compared to only 4 nucleotides in DNA) and the energy cost of unfolding a protein to sequence it.[38]

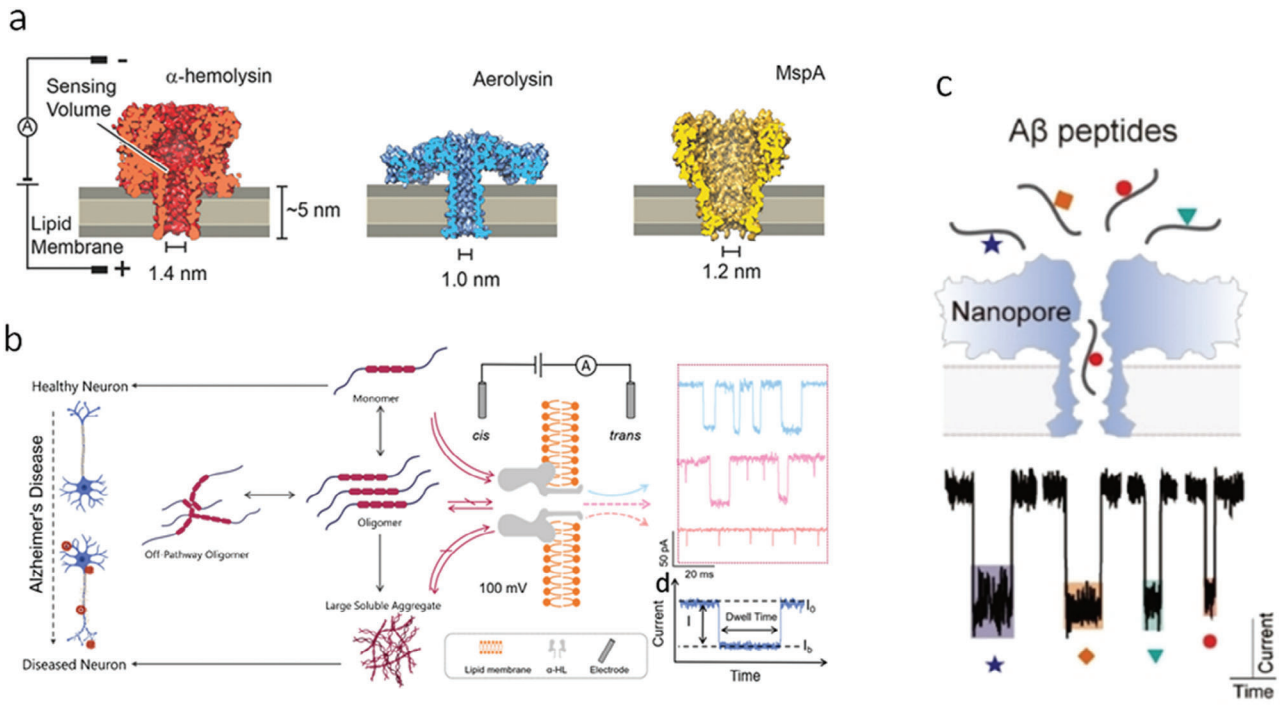

Figure 4. a) Example of different biological nanopores. Figure adapted from.[28a] Copyright 2018, Wiley b) Detection of the different species formed during the aggregation of Aβ with an a-hemolysin nanopore. Figure adapted from.[40] Copyright 2021, Elsevier c) Detection and discrimination of Aβ 1-42 peptides varying by only one amino acid in their sequence by an aerolysin nanopore. Figure adapted from.[51] Copyright 2022, Wiley.

Nevertheless, outstanding results have recently been reported for the identification of short peptides and the detection of single amino acid substitutions.[39]

The study of biological nanopores has attracted considerable interest because of their potential to detect monomers and oligomers smaller than a few nanometers. For example, α-hemolysin has been used to study the oligomerization process of β-amyloid (Aβ) 1–40. Monomers induce current blockades upon translocation, whereas oligomers larger than the nanopore size exhibit bumping events without translocation (Figure 4b).[40] These bump events are characterized by shorter durations and smaller amplitudes of current blockade than translocation events. Subsequent research conducted by the same group demonstrated the modulation of Aβ 1–40 aggregation by acetylcholinesterase (AchE), a molecule suspected to play a role in Alzheimer's disease, as indicated by changes in the duration and amplitude of current blockade.[41] Furthermore, using the same nanopore, the cleavage of the Aβ 10–20 peptide species was detected, and the kinetic constants of enzymatic degradation were determined through a detailed analysis of the parameters of the blocking events.[42] Another study compared the frequency and amplitude of current blockade events in the absence and presence of δ-cyclodextrine. The results indicated an increase in the number of bumping events due to the formation of aggregates too large to translocate into the nanopore.[43] The blocking parameters (amplitude, duration, and frequency) induced by two Aβ truncated peptides, Aβ 25–35, and Aβ 35-25, were also analyzed. The study revealed a large current blockade for the Aβ 25–35 peptide, which is attributed to its β-sheet structure, whereas a small current blockade was observed for the Aβ 35-25 peptide, which was interpreted as an α-helix/loop structure. In addition, the decrease in current blockade over time demonstrated the pro-aggregative behavior of Aβ 25–35, in contrast to Aβ 35-25.[44]

It is widely recognized that certain metal ions can accelerate aggregation, a process that has been extensively studied.[45] In this context, the interactions between the Aβ1-16 peptide and various metal ions, including Cu^{2+}, Zn^{2+}, Fe^{2+}, and Al^{2+}, were investigated using a biological nanopore system.[46] In the presence of metal cations, a decrease in the frequency, duration, and amplitude of the current blockade was observed, with the most significant effect observed for Cu^{2+}. Further analysis of the current blockade allowed the determination of the dissociation constants between the peptide and the cations, revealing a sequence of $Cu^{2+}<Zn^{2+}<Fe^{2+}<Al^{2+}$. Another study investigated the interaction between the HIS13 of the Aβ1-16 peptide and Cu^{2+}.[47] The event frequency indicated that the association and dissociation constants of the peptide were higher for rat Aβ1-16 than for human Aβ1-16, which was attributed to an ion-induced conformational change in the peptide. Further investigations also examined the influence of chirality on the interaction between wild-type (or variant form) Aβ1-16 peptides and Cu^{2+} by determining the different dissociation constants for the different peptide sequences.[48]

Recently, the reversible binding kinetics of α-synuclein in α-hemolysin nanopores were investigated by analyzing current blockade. This approach allowed characterization of the influence of metal ions, such as Cu^{2+} and Zn^{2+}, on the dynamics of α-synuclein interactions with biological membranes.[49] The nanopore, formed by a mutant of aerolysin, provides excellent resolution for peptide analysis, as demonstrated by the mapping of all amino acids and the characterization of post-translational modifications of peptides.[38a,50] The use of this nanopore made it possible to distinguish β-peptides with a single amino acid substitution in their sequence (Figure 4c), thereby[51] allowing the detection of typical family mutations. This nanopore was used for the fragment analysis of α-synuclein after protease treatment. The ability to identify single amino acid replacements and the demonstration of good agreement with mass spectroscopy analysis overcomes the main limitation of biological nanopores for protein analysis, and represents a significant step forward in protein sequencing by nanopores.[50b,52]

In general, biological nanopores are characterized by their excellent reproducibility and high precision, due to their perfectly controlled geometry.[43] In addition, their internal structure can be modified through directed mutagenesis to optimize properties, such as the distribution of electrical charges involved in analyte capture[53] or the constriction involved in analyte reading.[54] However, biological nanopores have a diameter limitation ≈4 nm, which makes them unsuitable for characterizing amyloid aggregates that are several tens of nanometers in size and organized in sheet-β, although they can be detected by bumping events. Therefore, it is necessary to use artificial nanopores to overcome this size limitation.

2.2. Solid-State Nanopore with Low Aspect Ratio For "Prion-Like" Protein Sensing

Solid-state nanopores drilled directly into silicon-based thin films have emerged as an alternative to biological nanopores since the early 2000s.[55] These nanopores are produced by dielectric breakdown (CBD), drilling with a focused ion beam (FIB), or electron beam (TEM). They have a low aspect ratio, defined as the ratio of the length to diameter of the nanopore (**Figure 5a**), which provides high precision for spherical structures. The diameter of these nanopores can be adjusted from a few nanometers to ten micrometers, depending on the thickness and chemical composition of the thin film and the drilling technique used. Their properties can be easily tuned by grafting or adsorbing molecules or polymers.[56] Although they are less reproducible and precise than biological nanopores, solid-state nanopores can be used to detect protein aggregates. Silicon nitride (SiN) nanopores have good resolution for this purpose, but non-specific adsorption of amyloid is a major drawback that can be overcome by surface functionalization. This involves the use of hydrophilic chemical moieties that reduce adsorption, prevent pore clogging, increase wettability, and extend the lifetime of nanopores.[28a,57] In a pioneering work, a double phospholipid bilayer was adsorbed on SiN to avoid clogging of nanopores. Analysis of β-amyloid 1–42 aggregations over 72 h of incubation revealed a decrease in the frequency of events, while the amplitude of the current blockade increased, suggesting fewer but larger aggregates in the solution over time (Figure 5b).[57] Using similar nanopore functionalization, the same group proposed a simple but elegant

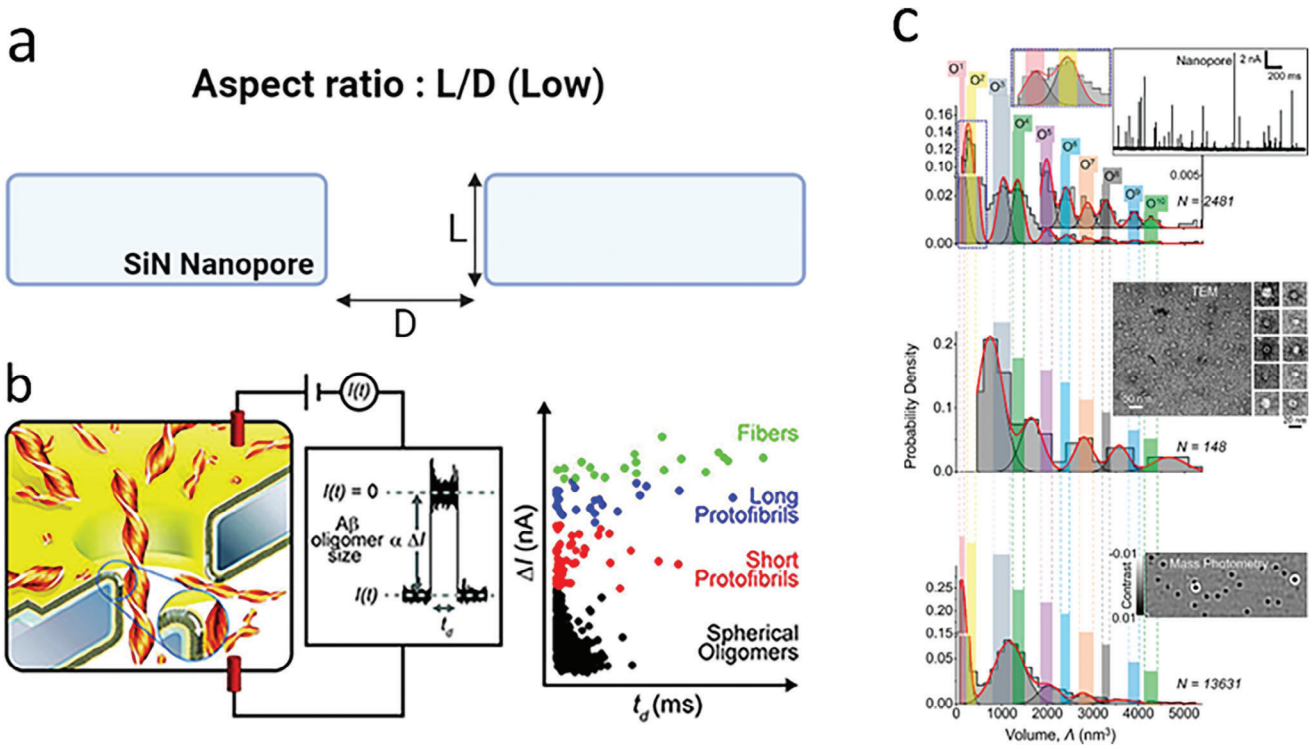

Figure 5. a) Schematic of a SiN nanopore with a low aspect ratio. b) Detection of the different aggregates formed during aggregation of the Aβ 1-42 peptide by SiN nanopore. With increasing incubation time, blocking events have larger amplitudes and longer timescales, suggesting the formation of increasingly large aggregates. Figure adapted from.[94] Copyright, 2012, American Chemical Society c) Estimated volumes of oligomers formed following α−synuclein aggregation from measured ΔI/I blocking events. Estimated volumes correlate well with microscopic characterization techniques. Figure adapted from.[58] Copyright 2023, American Chemical Society.

geometric model to estimate the volume and shape of amyloids using the obtained blocking parameters.[28b,c]

$$\frac{\Delta I}{I_0} = \frac{\gamma \Lambda}{\pi . rp^2 \, (lp + 1.6rp)} \, S\left(\frac{rp}{2Rh}\right) \quad (1)$$

Where Λ is the analyte volume (m^3), γ is a form factor and Rh is the hydrodynamic radius of the protein. rp and lp correspond to the pore radius and length respectively. This model was used to study the size and shape of α-synuclein aggregates in a complex mixture. The results of the nanopore analysis showed that the oligomers were composed of 2 to 122 monomers, corresponding to spheres of 30 nm diameter. This is in good agreement with the results obtained from transmission electron microscopy (TEM) and mass photometry imaging (Figure 5c).[58] Such an approach is also suitable to determine the number of oligomers of ß-lactoglobulin using a dsDNA molecule as a reference.[59]

Using SiN nanopores coated with Tween-20, the oligomerization of both wild-type and two variant forms (E46K and A30P) of α-synuclein was studied.[60] Following a six-day incubation period, a marked increase in the size and frequency of current blockages was observed in the mutants. Furthermore, the accelerated aggregation process exhibited by the A30P variant compared to the E46K underscores the pro-aggregative nature of both variants over the wild-type form.[61] In another study, researchers identified a multimodal distribution of the current blockade amplitude, which was attributed to the presence of four different intermediates during the aggregation process of α-synuclein. Based on these findings, the authors proposed a mechanism involving the consumption of "small oligomers" to produce larger structures. However, as these results have yet to be validated, further experimental evidence is needed to substantiate this claim.[62]

The use of SiN nanopores subjected to Pirhana oxidation is an effective method for the detection of unfolded monomers, dimers, trimers, and tetramers formed by lysozyme. This method has been found to correlate well with characterization data obtained by electrophoresis, providing a reliable means of characterizing oligomer formation.[63] Functionalization with a polyethylene glycol (PEG) chain by silanization directly after surface oxidation is also a suitable strategy for the detection of protein aggregates. Using this method, the correlation between the amplitude of the current blockade and size of the aggregate (amorphous for BSA vs structured as β-sheets for β-lactoglobulin and lysozyme) was established.[64] Recently, fibrils formed by β-lactoglobulin have been characterized at different pH values (7 and 4.6) under partial and non-denaturing conditions.[65] The aggregate species were found to be between 10 and 100 nm in length and 1 and 5 nm in diameter, consistent with atomic force microscopy and dynamic light scattering (DLS) characterization. In addition, this study highlights the formation of larger aggregates at acidic pH, in agreement with the literature.[66] Functionalization with L-dopamine, a neurotransmitter known for its anti-bioadhesive properties, is also a suitable approach to reduce nanopore fouling. Using a CDB-drilled nanopore of ≈5 nm diameter, the

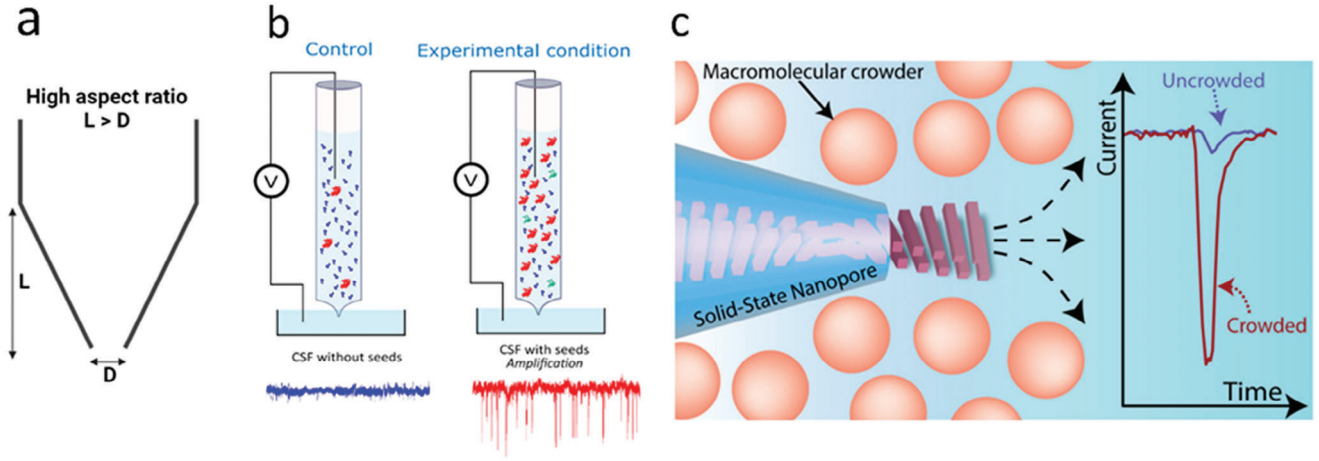

Figure 6. a) Schematic of a nanopipette with a high aspect ratio. b) Detection of aggregation seeding by a small amount of aggregation by RT-FaST. The control (blue) shows no blocking events, while the seeded condition (red) does. Figure adapted from.[76] Copyright, 2023, American Chemical Society c) Increase in signal-to-noise ratio by a factor of 6 after addition of polyethylene glycol to clog the system. PEG clogging enabled detection and discrimination of unfragmented and fragmented $\alpha-$synuclein fibers. Figure adapted from.[75] Copyright, 2020, American Chemical Society.

monomer-to-dimer ratio of α-synuclein WT and A53T was determined. This approach also showed a higher degree of polymorphism and larger size of β-amyloid E22Δ (Osaka variant) aggregates after a short incubation with β-amyloid WT oligomers with fibrils.[67]

Several reports have demonstrated the utility of functionalized solid-state nanopores for studying the early stages of protein and peptide aggregation. The high resolution of these nanopores has allowed the determination of the number of monomers within oligomers, albeit assuming their volume. However, there are several limitations to the practical application of these nanopores in real life. First, the short lifetime of the SiN nanopores precludes continuous measurements over long periods of time.[68] Although suitable for the study of spherical structures, such as folded proteins, their efficiency in detecting fibrils remains controversial, as reports of translocation, bumping, or clogging of nanopores have been documented.[57,63] In addition, the reduction of protein or peptide interactions with the inner wall of the nanopore surface can decrease the frequency of events, as translocation exceeds the sampling rate of the amplifier.[33d]

2.3. "Prion-Like" Protein Sensing Using Nanopipette

The nanopipette manufacturing process involves heating a quartz capillary with a focused laser while pulling it in opposite directions. This process results in the production of two nanopipettes with diameters that can be tuned from nanometers to micrometers depending on the pulling parameters and capillary geometry.[69] The production of nanopipettes is less expensive than that of SiN nanopores, as quartz capillaries are commercially available in the price range of $1 to $2.[70] The conical geometry of the nanopipettes allows amyloid fibrils to be detected in two ways. The traditional method involves detection from the outside to the inside of the nanopipette, which is suitable for oligomers and low aspect ratio nanopores such as SiN. The opposite method involves the detection of fibrils from the inside to the outside of the nanopipette, due to the conical geometry, which progressively orients the fibrils along the nanopore (**Figure 6**a).

Nanopipettes have been used to detect various protein aggregates, including amyloids and prions, often without functionalization.[71] They have been used to study the aggregation of lysozyme, and it was observed that the frequency and amplitude of current blockade increased, suggesting the formation and growth of aggregates with incubation.[72] This finding was confirmed by atomic force microscopy images that displayed a mixture of oligomers and fibers. However, this study did not show a correlation between blockade amplitudes and the volume or structure of the species detected. Aggregation of Aβ1-42 was monitored using nanopipettes with a diameter of ≈30 nm.[73] Current blockade varied with the incubation time. Initially, current enhancement with a short duration was attributed to the translocation of monomers due to their charge, which drove mobile counterions inside the nanopore. This was followed by a long-duration current blockade, which was interpreted as a transient adsorption of the formed oligomers on the nanopore surface. Finally, with the incubation time, small and short current blockages were attributed to the bumping of fibrils that were too large to enter the nanopore.

The strategy of introducing amyloid samples into the pipette allowed the detection of both oligomer and fibril translocation. This was demonstrated using a set of $\beta-$1-42 fibrils produced in the presence of EGCG and then sonicated at different times and energy levels to serve as a calibration standard. A good correlation was found between the current blockade amplitude and the TEM characterization, which was analyzed using a geometric model (Equations 2 and 3).[68] Although the study concluded that the nanopore was unable to discriminate fibers with lengths longer than 80 nm, it was suitable for characterizing oligomer polymorphism through the analysis of the amplitude distribution.[74]

$$\frac{\Delta I}{I_0} = 1 - R_0/R_{max} \quad (2)$$

$$R_{max} = \frac{1}{G_{m_i n}} = \frac{1}{k\pi}\left(\frac{1}{2.a.r_{amy}}\log\left(\frac{\left(a.L_{amy}+r_t-r_{amy}\right)\left(r_t+r_{amy}\right)}{\left(a.\ L_{amy}+r_t+r_{amy}\right)\left(r_t-r_{amy}\right)}\right) + \frac{l_p-\ L_{amy}}{\left(r_t+aL_{amy}\right)r_b}\right) \quad (3)$$

where R_{max} is the resistance of the pore when the amyloid is inside and R_0 is the resistance in the absence of the amyloid, $r_{amy,}$ and L_{amy} are the radius and length of the amyloid respectively, κ is the conductivity of the solution, $r_{t,}$ and r_b are the radii of the tip and long side of the nanopore respectively.

Subsequent studies using α-synuclein oligomers have proposed an alternative geometric model that allows direct determination of oligomer volume from the amplitude of the current blockade (Saly reference). To increase the frequency of events by optimizing the signal-to-noise ratio, it is possible to add PEG to the reservoir outside the nanopipette. Using this crowding, the fibrils formed by α-synuclein before or after ultrasound fragmentation were distinguished by the amplitude of the current blockade.[75]

Recent investigations have directly monitored aggregation of Aβ 1-42 within the reservoir of a nanopipette, either in the absence or presence of a small amount of pre-formed aggregates. The results showed that current blockages were only observed in conditions seeded with pre-formed aggregates after an incubation period of 3 h, allowing the differentiation between samples containing pre-formed aggregates and control samples (Figure 6b).[76] These findings were observed in buffer solutions, as well as in cerebrospinal fluid (4% v/v, cephalospinal fluid). Using the same methodology, the same research group demonstrated that this technique could be applied to quantify pre-formed aggregates of α-synuclein.[77] This method, called Real-Time Fast Amyloid Seeding and Translocation (RT-FasT), is similar to RT-QuIC, a current diagnostic tool for early detection of aggregates. RT-FasT significantly reduces the amount of monomer required and the incubation time by several orders of magnitude, paving the way for the development of early diagnostic tools using nanopipettes.[50a] Alternative strategies have been considered for diagnostic applications. One approach is to concentrate Aβ 1-42 oligomers in a membrane functionalized with an antibody combined with an ionic diode to confirm their binding. Oligomer detection was performed after washing the membrane with a nanopipette.[78] Two recent strategies have been reported to specifically bind α-synuclein oligomers to DNA strands and detect the complex using a nanopipette. In the first approach, the oligomer is bound to a DNA barcode, enabling the identification of specific types of oligomers through quantitative detection. This method was applied to early drug discovery, demonstrating performance comparable to other single-molecule techniques.[79] In the second approach, a DNA carrier was designed to specifically bind α-synuclein oligomers, with the presence of oligomers modifying the shape of the nanopipette's current blockage.[80] Notably, this method was applied to cerebrospinal fluid (CSF) biofluid, enabling the discrimination of patient samples with Parkinson's disease from controls.

The advantages of nanopipettes for the detection of protein aggregates have been demonstrated in numerous studies. A notable advantage of this method is the simplicity and reproducibility of its preparation.[81] Only a small volume of a few tens of microlitres is required to fill a nanopipette, which is particularly advantageous when studying expensive amyloid samples or patient-derived samples. In addition, the stability of nanopipettes allows for the aggregation kinetics to be monitored over an extended period of several hours. However, due to their geometry, the resolution of nanopipettes is lower than that of SiNs, and the analysis of complex mixtures requires the use of multiple nanopipettes with different diameters to probe each oligomer population, as recently demonstrated by our group.[82]

2.4. "Prion-Like" Protein Sensing Using Polymer Nanopore

Polymer nanopores with high aspect ratios are a class of synthetic nanopores developed in the early 2000s.[83] The principle behind their creation involves two steps: In the first step, a polymer film, such as polycarbonate (PC) or polyethylene terephthalate (PET) is irradiated with a heavy swift ion with energy in the MeV/nucleon range[84] to damage the material. In a second step, the irradiated film was chemically etched to form nanopores. By manipulating the experimental conditions of etching, such as asymmetry, concentration of the etching agent, temperature, time, and activation time of surfactant addition, the size and shape of the nanopore can be tuned (**Figure 7a**).[85] These nanopores have the advantage of being easily functionalized in aqueous solutions and can be filled with aqueous solutions during the chemical etching process, resulting in their stability for several weeks. However, due to their high aspect ratio, their resolution is lower than that of nanopipettes and SiNs. In addition, for asymmetric geometries, there is a significant disparity in the nanopore size under the same etching conditions.

Conical polyethylene terephthalate (PET) nanopores functionalized with PEG have been used to distinguish different populations of β-lactoglobulin aggregates at different incubation times under acidic conditions.[68] In addition, these nanopores demonstrated the pro-aggregative effects of dextran and ethanol, and the anti-aggregative effects of curcumin, in agreement with previous literature.[86] Because of their stability, nanopores were also used to investigate the enzymatic degradation of β-lactoglobulin by trypsin, which resulted in a decrease in amplitude and event frequency, indicating the formation of smaller intermediates. In contrast, degradation by pepsin at pH 2 showed reaggregation, which was thought to be caused by a seeding mechanism once the enzyme was fully degraded. the data collected by the nanopores were used to determine the kinetic constants of the enzymatic degradation.[87] Similar nanopores were used to demonstrate the pro-aggregative effect of an amino acid substitution in the tau protein (P301L) compared to the wild-type during aggregation in the presence of heparin.[88] Different populations, including monomers, oligomers, and fibrils, were identified to determine the aggregation kinetic constants of each population. In addition, the study of current blockade fluctuations indicated that the mutation promoted aggregate fragmentation compared with wild-type aggregates. The early phase of aggregate formation for the β-amyloid (Aβ) 1–42 peptides was characterized using a conical etched trace nanopore with a diameter of 5 nm and an inner wall coated with PEG chains (Figure 7b).[89] In this study, we demonstrated the pro-aggregative effects of pyrimethanil, a

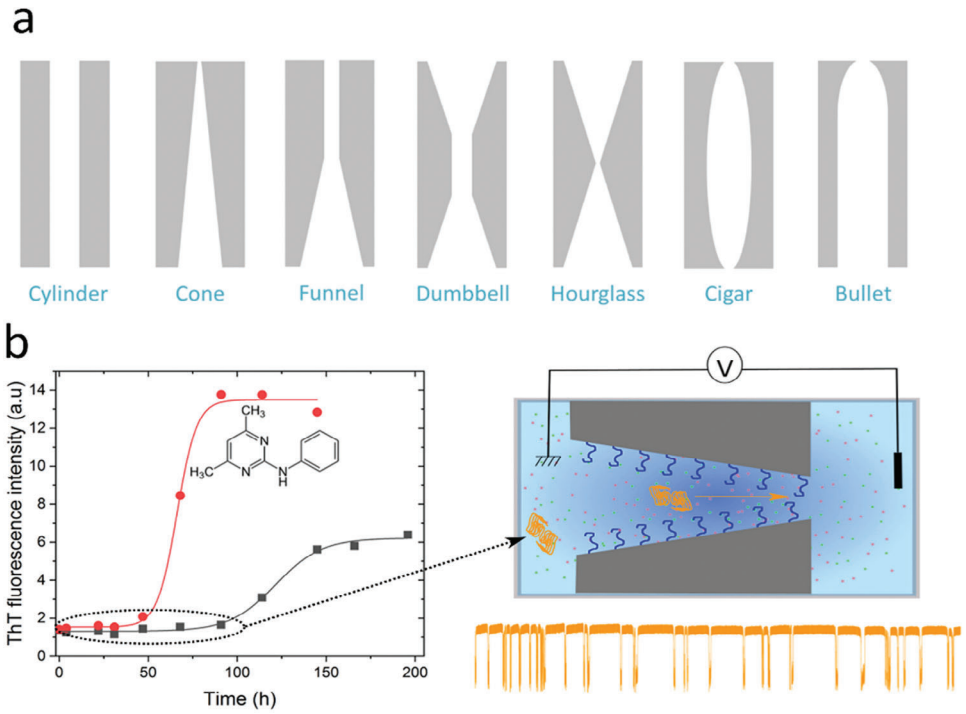

Figure 7. a) Schematic diagram of the different geometries that can be obtained with etched trace nanopore technology, depending on the experimental aperture conditions. b) Left, aggregation kinetics monitored by ThT in the absence (black) and presence (red) of pyrimethanil. Samples formed during the early phase (circled in dotted black) were analyzed by conical etched trace nanopore (right of Figure). Figure adapted from.[89] Copyright, 2021, Elsevier.

fungicide commonly found in organic agriculture and drinking water. In addition, the effects of geometry and crowding at the tip of the pore were compared for amyloid fibrils of different lengths.[90] Similar to the nanopipette, crowding was found to improve the signal-to-noise ratio, whereas the bullet-shaped geometry was better for differentiating between fibrils.[75]

3. Conclusion and Outlook

Nanopores provide a relevant platform for the detection and characterization of amyloids due to their versatility. Biological nanopores can detect monomers and oligomers, allowing the study of protein folding in the presence of metal ions, enzymatic degradation, and aggregation. The high-precision structure of nanopores allows characterization of single amino acid substitutions. The recent advancement in biological nanopores, which can now distinguish a single amino-acid modification such as mutation or phosphorylation, has the potential to rapidly analyze the mutation or phosphorylation of aβ peptide or α-synuclein. The ability to precisely size small peptides also allows for the measurement of the ratio aβ42/aβ40, a relevant indicator for clinical assays. However, the main drawback of biological nanopores is their small diameter, <4 nm, which limits their ability to study larger oligomers and fibrils and is therefore not suitable for the characterization of soluble oligomers.

Synthetic nanopores, on the other hand, are promising tools for the study of aggregation mechanisms due to their tunable diameter and functionalization. The in situ, label-free detection of single-molecule amyloids offers the potential to discriminate between different amyloid populations that form during the lag phase of aggregation. Geometric models can be used to estimate the structural characteristics of the detected oligomers using the current blockade parameters. In addition, nanopores are the only method that allows the detection of amyloids under continuous measurement, providing information on the size and shape of the myriad of protein assemblies. This unique measurement combines information from multiple techniques and offers a promising way to improve our understanding of protein misfolding and aggregation, particularly through the characterization of different proteomorphs. Selecting a set of nanopores with varying diameters allowed mapping of all species generated during the early stages. This opens up numerous opportunities for the development of multiplex platforms to investigate the effects of drugs and to create new therapies. With further development, particularly the precise calibration of the capture rate with oligomer concentration, nanopores could prove to be a suitable tool for quantitative analysis, especially following amplification. In addition to its potential application in diagnosis, the RT-FAST assay could also provide a new element in understanding secondary nucleation. However, there are several shortcomings to the use of solid-state nanopores. The analysis of complex mixtures can induce interference owing to the translocation of other compounds, requiring a purification step prior to nanopore analysis or the use of a carrier. The nanopore lifetime and possibility of reusing a nanopore several times are also important considerations. Nanopores with low aspect ratios that offer the best resolution for characterizing oligomers are not stable enough over time, and the success rate of experiments is low, especially when

surface functionalization is involved. Polymer nanopores can be used to address this stability problem; however, they fail to discriminate small oligomers with a suitable relationship to draw a precise map of their composition. The nanopipette is likely the best compromise in terms of resolution and lifetime, as demonstrated by the most advanced results in this field. Machine learning approaches can further enhance data analysis and assignment of signal shapes to oligomer structures.as demonstrated in the analysis of other glycosaminoglycans,[91] viruses,[92] and proteins.[93]

The most critical challenge for diagnostic applications appears to be the development of appropriate methods to detect amyloid in cerebrospinal fluid (CSF). Recent demonstrations using CSF have suggested that this is a feasible approach, and the use of amplification and DNA barcoded carriers offers promise for future applications. The application of nanopore technology holds great promise for enhancing existing methods that rely on amplification, particularly in terms of reducing the analysis time. This is due to the ability of the technology to detect early-stage oligomers, as well as the requirement of fewer samples for each analysis. However, further development and optimization are necessary to fully realize the potential of this technology, as only pioneering work has thus far demonstrated its potential.

Acknowledgements

This work was funded by the Agence Nationale de la Recherche (ANR-19-CE42-0006, NanoOligo).

Conflict of Interest

The authors declare no conflict of interest.

Keywords

amyloid fibers, nanopore, prion-like proteins oligomers, single-molecule techniques

Received: January 12, 2024
Revised: March 10, 2024
Published online:

[1] C. A. Ross, M. A. Poirier, *Nat. Med.* **2004**, *10*, S10.
[2] a) A. M. Morris, M. A. Watzky, R. G. Finke, *Biochim. Biophys. Acta* **2009**, *1794*, 375; b) S. Linse, *Pure Appl. Chem.* **2019**, *91*, 211; c) M. Sakono, T. Zako, *FEBS J.* **2010**, *277*, 1348.
[3] P. Arosio, T. P. J. Knowles, S. Linse, *Phys. Chem. Chem. Phys.* **2015**, *17*, 7606.
[4] M. Muschol, W. Hoyer, *Front. Mol. Biosci.* **2023**, *10*, 1120416.
[5] V. H. Finder, R. Glockshuber, *Neurodegener. Dis.* **2007**, *4*, 13.
[6] a) G. M. Shankar, S. Li, T. H. Mehta, A. Garcia-Munoz, N. E. Shepardson, I. Smith, F. M. Brett, M. A. Farrell, M. J. Rowan, C. A. Lemere, C. M. Regan, D. M. Walsh, B. L. Sabatini, D. J. Selkoe, *Nat. Med.* **2008**, *14*, 837; b) D. M. Walsh, A. Lomakin, G. B. Benedek, M. M. Condron, D. B. Teplow, *J. Biol. Chem.* **1997**, *272*, 22364; c) A. Sandberg, L. M. Luheshi, S. Söllvander, T. Pereira de Barros, B. Macao, T. P. J. Knowles, H. Biverstål, C. Lendel, F. Ekholm-Petterson, A. Dubnovitsky, L. Lannfelt, C. M. Dobson, T. Härd, *Proc. Natl. Acad. Sci.* **2010**, *107*, 15595.
[7] a) M. Wolff, D. Unuchek, B. Zhang, V. Gordeliy, D. Willbold, L. Nagel-Steger, *PLoS One* **2015**, *10*, 0127865; b) F. Hasecke, T. Miti, C. Perez, J. Barton, D. Schölzel, L. Gremer, C. S. R. Grüning, G. Matthews, G. Meisl, T. P. J. Knowles, D. Willbold, P. Neudecker, H. Heise, G. Ullah, W. Hoyer, M. Muschol, *Chem. Sci.* **2018**, *9*, 5937.
[8] a) A. J. Dear, G. Meisl, A. Šarić, T. C. T. Michaels, M. Kjaergaard, S. Linse, T. P. J. Knowles, *Chem. Sci.* **2020**, *11*, 6236; b) A. J. Dear, T. C. T. Michaels, G. Meisl, D. Klenerman, S. Wu, S. Perrett, S. Linse, C. M. Dobson, T. P. J. Knowles, *Proc. Natl. Acad. Sci.* **2020**, *117*, 12087; c) T. C. T. Michaels, A. Šarić, S. Curk, K. Bernfur, P. Arosio, G. Meisl, A. J. Dear, S. I. A. Cohen, C. M. Dobson, M. Vendruscolo, S. Linse, T. P. J. Knowles, *Nat. Chem.* **2020**, *12*, 445.
[9] S. I. A. Cohen, S. Linse, L. M. Luheshi, E. Hellstrand, D. A. White, L. Rajah, D. E. Otzen, M. Vendruscolo, C. M. Dobson, T. P. J. Knowles, *Proc. Natl. Acad. Sci.* **2013**, *110*, 9758.
[10] H. LeVine, *Protein Sci.* **1993**, *2*, 404.
[11] a) G. Liu, J. C. Gaines, K. J. Robbins, N. D. Lazo, *ACS Med. Chem. Lett.* **2012**, *3*, 856; b) L. Khemtemourian, F. Antoniciello, B. R. Sahoo, M. Decossas, S. Lecomte, A. Ramamoorthy, *Chem. Phys. Lipids* **2021**, *237*, 105083; c) T. K. Karamanos, A. P. Kalverda, G. S. Thompson, S. E. Radford, *Prog. Nucl. Magn. Reson. Spectrosc.* **2015**, *88–89*, 86; d) E. E. Cawood, T. K. Karamanos, A. J. Wilson, S. E. Radford, *Biophys. Chem.* **2021**, *268*, 106505.
[12] M. A. Wälti, F. Ravotti, H. Arai, C. G. Glabe, J. S. Wall, A. Böckmann, P. Güntert, B. H. Meier, R. Riek, *Proc. Natl. Acad. Sci.* **2016**, *113*, E4976.
[13] P. Juszczyk, A. S. Kołodziejczyk, Z. Grzonka, *J. Pept. Sci.* **2009**, *15*, 23.
[14] a) R. Sarroukh, E. Goormaghtigh, J.-M. Ruysschaert, V. Raussens, *Biochim. Biophys. Acta* **2013**, *1828*, 2328; b) G. Zandomeneghi, M. R. H. Krebs, M. G. McCammon, M. Fändrich, *Protein Sci.* **2004**, *13*, 3314.
[15] a) S. Bonhommeau, D. Talaga, J. Hunel, C. Cullin, S. Lecomte, *Angew. Chem.* **2017**, *129*, 1797; b) D. Talaga, G. S. Cooney, V. Ury-Thiery, Y. Fichou, Y. Huang, S. Lecomte, S. Bonhommeau, *J. Phys. Chem. B* **2022**, *126*, 5024.
[16] a) M. Bouchard, J. Zurdo, E. J. Nettleton, C. M. Dobson, C. V. Robinson, *Protein Sci.* **2000**, *9*, 1960; b) M. Bartolini, C. Bertucci, M. L. Bolognesi, A. Cavalli, C. Melchiorre, V. Andrisano, *ChemBioChem* **2007**, *8*, 2152.
[17] S. Kumar, J. B. Udgaonkar, *Current Science* **2010**, *98*, 639.
[18] S. Wennmalm, V. Chmyrov, J. Widengren, L. Tjernberg, *Anal. Chem.* **2015**, *87*, 11700.
[19] a) A. Bhumkar, C. Magnan, D. Lau, E. S. W. Jun, N. Dzamko, Y. Gambin, E. Sierecki, *Angew. Chem. Int. Ed.* **2021**, *60*, 11874; b) S. Balme, J.-M. Janot, P. Déjardin, E. N. Vasina, P. Seta, *J. Membr. Sci.* **2006**, *284*, 198; c) A. Tiiman, J. Jarvet, A. Gräslund, V. Vukojević, *Biochemistry* **2015**, *54*, 7203; d) K. Garai, R. Sureka, S. Maiti, *Biophys. J.* **2007**, *92*, L55.
[20] a) M. Baba, S. Nakajo, P. H. Tu, T. Tomita, K. Nakaya, V. M. Lee, J. Q. Trojanowski, T. Iwatsubo, *Am J Pathol* **1998**, *152*, 879; b) M. Owczarz, P. Arosio, *Biophys. J.* **2014**, *107*, 197; c) E. Hellstrand, B. Boland, D. M. Walsh, S. Linse, *ACS Chem. Neurosci.* **2010**, *1*, 13.
[21] a) M. Schmidt, **2009**; b) M. Schmidt, A. Rohou, K. Lasker, J. K. Yadav, C. Schiene-Fischer, M. Fändrich, N. Grigorieff, *Proc. Natl. Acad. Sci.* **2015**, *112*, 11858.
[22] A. Parbhu, H. Lin, J. Thimm, R. Lal, *Peptides* **2022**, *23*, 1265.
[23] M. Gregori, V. Cassina, D. Brogioli, D. Salerno, L. de Kimpe, W. Scheper, M. Masserini, F. Mantegazza, *Eur. Biophys. J.* **2010**, *39*, 1613.
[24] T. Watanabe-Nakayama, K. Ono, M. Itami, R. Takahashi, D. B. Teplow, M. Yamada, *Proc. Natl. Acad. Sci.* **2016**, *113*, 5835.
[25] a) J. J. Kasianowicz, E. Brandin, D. Branton, D. W. Deamer, *PNAS* **1996**, *93*, 13770; b) M. W. Loose, *Hum. Mol. Genet.* **2017**, *26*, R202.
[26] a) M. Ali, S. Nasir, Q. H. Nguyen, J. K. Sahoo, M. N. Tahir, W. Tremel, W. Ensinger, *J. Am. Chem. Soc.* **2011**, *133*, 17307; b) J. J. Kasianowicz, A. K. Balijepalli, J. Ettedgui, J. H. Forstater, H. Wang, H. Zhang, J. W.

F. Robertson, *Biochim. Biophys. Acta* **2016**, *1858*, 593; c) P. Waduge, R. Hu, P. Bandarkar, H. Yamazaki, B. Cressiot, Q. Zhao, P. C. Whitford, M. Wanunu, *ACS Nano* **2017**, *11*, 5706; d) S. Cabello-Aguilar, A. A. Chaaya, M. Bechelany, C. Pochat-Bohatier, E. Balanzat, J.-M. Janot, P. Miele, S. Balme, *Soft Matter* **2014**, *10*, 8413; e) N. Meyer, I. Abrao-Nemeir, J.-M. Janot, J. Torrent, M. Lepoitevin, S. Balme, *Adv. Colloid Interface Sci.* **2021**, 102561.

[27] a) J. E. Wharton, P. Jin, L. T. Sexton, L. P. Horne, S. A. Sherrill, W. K. Mino, C. R. Martin, *Small* **2007**, *3*, 1424; b) H. Bayley, C. R. Martin, *Chem. Rev.* **2000**, *100*, 2575.

[28] a) J. Houghtaling, J. List, M. Mayer, *Small* **2018**, *14*, 1802412; b) J. Houghtaling, C. Ying, O. M. Eggenberger, A. Fennouri, S. Nandivada, M. Acharjee, J. Li, A. R. Hall, M. Mayer, *ACS Nano* **2019**, *13*, 5231; c) E. C. Yusko, B. R. Bruhn, O. M. Eggenberger, J. Houghtaling, R. C. Rollings, N. C. Walsh, S. Nandivada, M. Pindrus, A. R. Hall, D. Sept, J. Li, D. S. Kalonia, M. Mayer, *Nat. Nanotechnol.* **2017**, *12*, 360.

[29] a) Y. Zhang, G. Wu, W. Si, J. Ma, Z. Yuan, X. Xie, L. Liu, J. Sha, D. Li, Y. Chen, *Nanoscale* **2017**, *9*, 930; b) Y. Ai, S. Qian, *Phys. Chem. Chem. Phys.* **2011**, *13*, 4060.

[30] a) N. Varongchayakul, J. Song, A. Meller, M. W. Grinstaff, *Chem. Soc. Rev.* **2018**, *47*, 8512; b) C. Raillon, P. Granjon, M. Graf, L. J. Steinbock, A. Radenovic, *Nanoscale* **2012**, *4*, 4916.

[31] S. Balme, M. Lepoitevin, L. F. Dumée, M. Bechelany, J.-M. Janot, *Soft Matter* **2017**, *13*, 496.

[32] A. Carlsen, V. Tabard-Cossa, *Proteomics* **2022**, *22*, 2100068.

[33] a) B. Cressiot, A. Oukhaled, G. Patriarche, M. Pastoriza-Gallego, J.-M. Betton, L. Auvray, M. Muthukumar, L. Bacri, J. Pelta, *ACS Nano* **2012**, *6*, 6236; b) M.-Y. Li, Y.-L. Ying, J. Yu, S.-C. Liu, Y.-Q. Wang, S. Li, Y.-T. Long, *JACS Au* **2021**, *1*, 967; c) S.-M. Lu, M.-Y. Li, Y.-T. Long, *J. Phys. Chem. Lett.* **2022**, *13*, 4653; d) J. Larkin, R. Y. Henley, M. Muthukumar, J. K. Rosenstein, M. Wanunu, *Biophys. J.* **2014**, *106*, 696.

[34] Y. Lin, Y.-L. Ying, X. Shi, S.-C. Liu, Y.-T. Long, *Chem. Commun.* **2017**, *53*, 11564.

[35] Y.-L. Ying, C. Cao, Y.-T. Long, *Analyst* **2014**, *139*, 3826.

[36] M. Dal Peraro, F. G. van der Goot, *Nat. Rev. Microbiol.* **2016**, *14*, 77.

[37] a) L. Payet, M. Martinho, M. Pastoriza-Gallego, J.-M. Betton, L. Auvray, J. Pelta, J. Mathé, *Anal. Chem.* **2012**, *84*, 4071; b) B. Cressiot, H. Ouldali, M. Pastoriza-Gallego, L. Bacri, F. G. van der Goot, J. Pelta, *ACS Sens.* **2019**, *4*, 530.

[38] a) H. Ouldali, K. Sarthak, T. Ensslen, F. Piguet, P. Manivet, J. Pelta, J. C. Behrends, A. Aksimentiev, A. Oukhaled, *Nat. Biotechnol.* **2020**, *38*, 176; b) F. Piguet, H. Ouldali, M. Pastoriza-Gallego, P. Manivet, J. Pelta, A. Oukhaled, *Nat. Commun.* **2018**, *9*, 966.

[39] a) H. Brinkerhoff, A. S. W. Kang, J. Liu, A. Aksimentiev, C. Dekker, *Science* **2021**, *374*, 1509; b) A. Stierlen, S. J. Greive, L. Bacri, P. Manivet, B. Cressiot, J. Pelta, *ACS Cent. Sci.* **2023**, *9*, 228.

[40] B. Lenhart, X. Wei, B. Watson, X. Wang, Z. Zhang, C. Li, M. Moss, C. Liu, *Sens. Actuators B* **2021**, *338*, 129863.

[41] N. Subramanian, B. Watson, C.-Z. Li, M. Moss, C. Liu, *Sens. Actuators Rep.* **2023**, *6*, 100170.

[42] Q. Zhao, R. S. S. de Zoysa, D. Wang, D. A. Jayawardhana, X. Guan, *J. Am. Chem. Soc.* **2009**, *131*, 6324.

[43] H.-Y. Wang, Y.-L. Ying, Y. Li, H.-B. Kraatz, Y.-T. Long, *Anal. Chem.* **2011**, *83*, 1746.

[44] Y.-X. Hu, Y.-L. Ying, Z. Gu, C. Cao, B.-Y. Yan, H.-F. Wang, Y.-T. Long, *Chem. Commun.* **2016**, *52*, 5542.

[45] a) P. Faller, *ChemBioChem* **2009**, *10*, 2837; b) C. Ha, J. Ryu, C. B. Park, *Biochemistry* **2007**, *46*, 6118.

[46] a) A. Asandei, S. Iftemi, L. Mereuta, I. Schiopu, T. Luchian, *J. Membr. Biol.* **2014**, *247*, 523; b) T. Luchian, Y. Park, A. Asandei, I. Schiopu, L. Mereuta, A. Apetrei, *Acc. Chem. Res.* **2019**, *52*, 267.

[47] A. Asandei, I. Schiopu, S. Iftemi, L. Mereuta, T. Luchian, *Langmuir* **2013**, *29*, 15634.

[48] I. Schiopu, S. Iftemi, T. Luchian, *Langmuir* **2015**, *31*, 387.

[49] J. Wu, T. Yamashita, A. D. Hamilton, S. Thompson, J. Luo, *Cell Rep. Phys. Sci.* **2023**, *4*, 101243.

[50] a) B. Cressiot, J. Pelta, *ACS Cent. Sci.* **2022**, *8*, 415; b) M. Afshar Bakshloo, S. Yahiaoui, M. Bourderioux, R. Daniel, M. Pastoriza-Gallego, J. J. Kasianowicz, A. Oukhaled, *ACS Chem. Neurosci.* **2023**, *14*, 2517.

[51] K.-L. Xin, Z.-L. Hu, S.-C. Liu, X.-Y. Li, J.-G. Li, H. Niu, Y.-L. Ying, Y.-T. Long, *Angew. Chem. Int. Ed.* **2022**, *61*, 202209970.

[52] M. Afshar Bakshloo, J. J. Kasianowicz, M. Pastoriza-Gallego, J. Mathé, R. Daniel, F. Piguet, A. Oukhaled, *J. Am. Chem. Soc.* **2022**, *144*, 2716.

[53] a) Y.-Q. Wang, C. Cao, Y.-L. Ying, S. Li, M.-B. Wang, J. Huang, Y.-T. Long, *ACS Sens.* **2018**, *3*, 779; b) S. Howorka, J. Nam, H. Bayley, D. Kahne, *Angew. Chem.* **2004**, *116*, 860.

[54] S. E. van der Verren, N. van Gerven, W. Jonckheere, R. Hambley, P. Singh, J. Kilgour, M. Jordan, E. J. Wallace, L. Jayasinghe, H. Remaut, *Nat. Biotechnol.* **2020**, *38*, 1415.

[55] a) M. Rahman, M. J. N. Sampad, A. Hawkins, H. Schmidt, *Lab Chip* **2021**, *21*, 3030; b) N. Li, S. Yu, C. C. Harrell, C. R. Martin, *Anal. Chem.* **2004**, *76*, 2025.

[56] a) S. W. Kowalczyk, T. R. Blosser, C. Dekker, *Trends Biotechnol.* **2011**, *29*, 607; b) M. Lepoitevin, T. Ma, M. Bechelany, J.-M. Janot, S. Balme, *Adv. Colloid Interface Sci.* **2017**, *250*, 195.

[57] E. C. Yusko, J. M. Johnson, S. Majd, P. Prangkio, R. C. Rollings, J. Li, J. Yang, M. Mayer, *Nat. Nanotechnol.* **2011**, *6*, 253.

[58] S. Awasthi, C. Ying, J. Li, M. Mayer, *ACS Nano* **2023**, *17*, 12325.

[59] M. C. Acharjee, B. Ledden, B. Thomas, X. He, T. Messina, J. Giurleo, D. Talaga, J. Li, *Sensors* **2024**, *24*, 81.

[60] X. Li, X. Tong, W. Lu, D. Yu, J. Diao, Q. Zhao, *Nanoscale* **2019**, *11*, 6480.

[61] K. Beyer, *Acta Neuropathol.* **2006**, *112*, 237.

[62] R. Hu, J. Diao, J. Li, Z. Tang, X. Li, J. Leitz, J. Long, J. Liu, D. Yu, Q. Zhao, *Sci. Rep.* **2016**, *6*, 20776.

[63] S. Balme, P. E. Coulon, M. Lepoitevin, B. Charlot, N. Yandrapalli, C. Favard, D. Muriaux, M. Bechelany, J.-M. Janot, *Langmuir* **2016**, *32*, 8916.

[64] N. Giamblanco, D. Coglitore, J.-M. Janot, P. E. Coulon, B. Charlot, S. Balme, *Sens. Actuators, B* **2018**, *260*, 736.

[65] M. C. Acharjee, B. Ledden, B. Thomas, X. He, *Sensors* **2024**, *24*, 81.

[66] a) J. M. Khan, A. Malik, F. M. Husain, M. J. Hakeem, A. S. Alhomida, *Polymers* **2022**, *14*, 395; b) J. K. Keppler, T. R. Heyn, P. M. Meissner, K. Schrader, K. Schwarz, *Food Chem.* **2019**, *289*, 223.

[67] I. Abrao-Nemeir, J. Bentin, N. Meyer, J.-M. Janot, J. Torrent, F. Picaud, S. Balme, *Chem. Asian J.* **2022**, *17*, 202200726.

[68] N. Giamblanco, D. Coglitore, A. Gubbiotti, T. Ma, E. Balanzat, J.-M. Janot, M. Chinappi, S. Balme, *Anal. Chem.* **2018**, *90*, 12900.

[69] a) P. Actis, A. C. Mak, N. Pourmand, *Bioanal. Rev.* **2010**, *1*, 177; b) P. Actis, O. Jejelowo, N. Pourmand, *Biosens. Bioelectron.* **2010**, *26*, 333.

[70] R. C. Mani, X. Li, M. K. Sunkara, K. Rajan, *Nano Lett.* **2003**, *3*, 671.

[71] W. Li, N. A. W. Bell, S. Hernández-Ainsa, V. V. Thacker, A. M. Thackray, R. Bujdoso, U. F. Keyser, *ACS Nano* **2013**, *7*, 4129.

[72] N. Martyushenko, N. A. W. Bell, R. D. Lamboll, U. F. Keyser, *Analyst* **2015**, *140*, 4882.

[73] R.-J. Yu, S.-M. Lu, S.-W. Xu, Y.-J. Li, Q. Xu, Y.-L. Ying, Y.-T. Long, *Chem. Sci.* **2019**, *10*, 10728.

[74] I. Abrao-Nemeir, N. Meyer, A. Nouvel, S. Charles-Achille, J.-M. Janot, J. Torrent, S. Balme, *Biophys. Chem.* **2023**, *300*, 107076.

[75] C. C. Chau, S. E. Radford, E. W. Hewitt, P. Actis, *Nano Lett.* **2020**, *20*, 5553.

[76] N. Meyer, J. Bentin, J.-M. Janot, I. Abrao-Nemeir, S. Charles-Achille, M. Pratlong, A. Aquilina, E. Trinquet, V. Perrier, F. Picaud, J. Torrent, S. Balme, *Anal. Chem.* **2023**, *95*, 12623.

[77] N. Meyer, J.-M. Janot, J. Torrent, S. Balme, *ACS Cent. Sci.* **2022**, *8*, 441.

[78] M. Moderne, I. Abrao-Nemeir, N. Meyer, J. Du, S. Charles-Achille, J.-M. Janot, J. Torrent, M. Lepoitevin, S. Balme, *Anal. Chim. Acta* **2023**, *1275*, 341587.
[79] S. E. Sandler, R. I. Horne, S. Rocchetti, R. Novak, N.-S. Hsu, M. Castellana Cruz, Z. Faidon Brotzakis, R. C. Gregory, S. Chia, G. J. L. Bernardes, U. F. Keyser, M. Vendruscolo, *J. Am. Chem. Soc.* **2023**, *145*, 25776.
[80] Y. Liu, X. Wang, G. Campolo, X. Teng, L. Ying, J. B. Edel, A. P. Ivanov, *ACS Nano* **2023**, *17*, 22999.
[81] X. Xu, D. Valavanis, P. Ciocci, S. Confederat, F. Marcuccio, J.-F. Lemineur, P. Actis, F. Kanoufi, P. R. Unwin, *Anal. Chem.* **2023**, *95*, 319.
[82] S. Charles-Achille, J.-M. Janot, B. Cayrol, S. Balme, *ChemBioChem* **2024**, *25*, 202300748.
[83] a) T. Ma, J.-M. Janot, S. Balme, *Small Methods* **2020**, *4*, 2000366; b) P. Apel, Y. E. Korchev, Z. Siwy, R. Spohr, M. Yoshida, Nuclear Instruments and Methods in Physics Research B **2001**, *184*, 337.
[84] D. Kaya, K. Keçeci, *J. Electrochem. Soc.* **2020**, *167*, 37543.
[85] a) P. Y. Apel, S. N. Dmitriev, *Adv. Nat. Sci: Nanosci. Nanotechnol.* **2011**, *2*, 13002; b) K. Froehlich, M. C. Scheuerlein, M. Ali, S. Nasir, W. Ensinger, *Nanotechnology* **2021**, *33*, 045301.
[86] a) S. Radbakhsh, G. E. Barreto, A. R. Bland, A. Sahebkar, *BioFactors* **2021**, *47*, 570; b) P. Semenyuk, L. Kurochkina, K. Barinova, V. Muronetz, *Polymers* **2020**, *12*, 537.
[87] N. Giamblanco, J.-M. Janot, A. Gubbiotti, M. Chinappi, S. Balme, *Small Methods* **2020**, *9*, 1900703.
[88] N. Giamblanco, Y. Fichou, J.-M. Janot, E. Balanzat, S. Han, S. Balme, *ACS Sens.* **2020**, *5*, 1158.
[89] N. Meyer, N. Arroyo, M. Baldelli, N. Coquart, J. M. Janot, V. Perrier, M. Chinappi, F. Picaud, J. Torrent, S. Balme, *Chemosphere* **2021**, *291*, 132733.
[90] N. Meyer, N. Arroyo, J.-M. Janot, M. Lepoitevin, A. Stevenson, I. A. Nemeir, V. Perrier, D. Bougard, M. Belondrade, D. Cot, J. Bentin, F. Picaud, J. Torrent, S. Balme, *ACS Sens.* **2021**, *6*, 3733.
[91] a) J. Im, S. Lindsay, X. Wang, P. Zhang, *ACS Nano* **2019**, *13*, 6308; b) K. Xia, J. T. Hagan, L. Fu, B. S. Sheetz, S. Bhattacharya, F. Zhang, J. R. Dwyer, R. J. Linhardt, *Proc. Natl. Acad. Sci.* **2021**, *118*, 2022806118.
[92] a) S. Hattori, R. Sekido, I. W. Leong, M. Tsutsui, A. Arima, M. Tanaka, K. Yokota, T. Washio, T. Kawai, M. Okochi, *Sci. Rep.* **2020**, *10*, 15525; b) M. Taniguchi, S. Minami, C. Ono, R. Hamajima, A. Morimura, S. Hamaguchi, Y. Akeda, Y. Kanai, T. Kobayashi, W. Kamitani, Y. Terada, K. Suzuki, N. Hatori, Y. Yamagishi, N. Washizu, H. Takei, O. Sakamoto, N. Naono, K. Tatematsu, T. Washio, Y. Matsuura, K. Tomono, *Nat. Commun.* **2021**, *12*, 3726; c) A. Arima, M. Tsutsui, T. Washio, Y. Baba, T. Kawai, *Anal. Chem.* **2021**, *93*, 215; d) A. Arima, I. H. Harlisa, T. Yoshida, M. Tsutsui, M. Tanaka, K. Yokota, W. Tonomura, J. Yasuda, M. Taniguchi, T. Washio, M. Okochi, T. Kawai, *J. Am. Chem. Soc.* **2018**, *140*, 16834.
[93] L. Reynaud, A. Bouchet-Spinelli, J.-M. Janot, A. Buhot, S. Balme, C. Raillon, *Anal. Chem.* **2021**, *93*, 7889.
[94] E. C. Yusko, P. Prangkio, D. Sept, R. C. Rollings, J. Li, M. Mayer, *ACS Nano* **2012**, *6*, 5909.

Nathan Meyer after completing his Bachelor's degree in Biochemistry followed by a Master's degree in Biophysics, Dr. Nathan Meyer earned his Ph.D. in 2023 under the guidance of Dr. Sébastien Balme and Dr. Joan Torrent (University of Montpellier). During his doctoral studies, Nathan specialized in optimizing nanopore technology for the detection and analysis of aggregates associated with the early stages of Alzheimer's and Parkinson's diseases. Currently, Dr. Meyer holds a postdoctoral position at the LAMBE laboratory (Cergy University) in the group of Pr. Juan Pelta and under the supervision of Dr. Benjamin Cressiot. His current research focuses on protein nanopores for the detection of biological peptides.

Joan Torrent his research interests cover various topics related to protein folding problems. He completed his Ph.D. at the University of Girona (Spain) in 2000, where he studied protein stability. As a postdoctoral fellow at Inserm (France), he studied amyloid formation under high pressure, providing a volumetric comprehension of the misfolding process. In 2006, he established his own research program as a Senior Scientist at Inserm. His research combines protein biochemistry and cell biology to identify factors that influence protein misfolding and aggregation, focusing on those that affect the morphology and neurotoxicity of amyloids and their autocatalytic propagation in the brain.

Sébastien Balme is associate professor of physical chemistry at the University of Montpellier. He obtained his Ph.D. in physical chemistry there in 2005 and, after a postdoc at the University of Geneva, returned in 2007. Since 2007 he has developed a research activity at the frontier between physical chemistry and biophysics. His efforts are focused on understanding the dynamic of (bio) macromolecules confined at the nanoscale, studying bio-inspired nanopores and membranes, and investigating the interaction between biomacromolecules at solid/liquid interface. Among his activities, he is developing nanopore sensors to understand protein aggregation and use them as tools for early disease diagnosis.

